CHEMISTRY
A EUROPEAN JOURNAL

FULL PAPER

DOI: 10.1002/chem.201301597

# Aggregation and Cooperative Effects in the Aldol Reactions of Lithium Enolates

Olatz Larrañaga,[a] Abel de Cózar,[a, b, c] F. Matthias Bickelhaupt,[c, d] Ronen Zangi,[a, b] and Fernando P. Cossío*[a]

**Abstract:** Density functional theory and Car–Parrinello molecular dynamics simulations have been carried out for model aldol reactions involving aggregates of lithium enolates derived from acetaldehyde and acetone. Formaldehyde and acetone have been used as electrophiles. It is found that the geometries of the enolate aggregates are in general determined by the most favorable arrangements of the point charges within the respective $Li_nO_n$ clusters. The reactivity of the enolates follows the sequence monomer ≫ dimer > tetramer. In lithium aggregates, the initially formed aldol adducts must rearrange to form more stable structures in which the enolate and alkoxide oxygen atoms are within the respective $Li_nO_n$ clusters. Positive cooperative effects, similar to allosteric effects found in several proteins, are found for the successive aldol reactions in aggregates. The corresponding transition structures show in general sofa geometries.

**Keywords:** aldol reaction · cooperative effects · density functional calculations · lithium aggregates · lithium enolates

## Introduction

The aldol reaction[1] is one of the most commonly used methods to generate C–C bonds in a convergent and stereocontrolled manner.[2] Although this reaction has been known since 1838,[3] there are many mechanistic aspects that are not completely understood. Despite its formal simplicity, the aldol reaction can occur with the assistance of different catalysts or promoters. These different methods can be grouped in two general families: enol derivatives or enolates,[4] and enamines.[5] Furthermore, these families have in turn their biochemical counterparts. Thus, type II aldolases[6] rely on zinc enolates, whereas type I aldolases[7] and catalytic monoclonal antibodies[8] are based on the α-activation of carbonyl compounds through the formation of enamines. An extension of this latter type of non-metal-assisted catalysis consists of the development of aldol reactions catalyzed by proline or proline-derived molecules.[9]

As far as the aldol reaction involving metallic enolates is concerned, a relevant issue is the nature of the reactive nucleophile, which is difficult to determine by kinetic investigations due to the very high reactivity of the nucleophilic species involved.[10] Different monomeric,[11] dimeric,[12] tetrameric,[13] and hexameric[14] enolate structures have been observed experimentally by means of colligative property measurements, X-ray, $^{7}Li$ and $^{13}C$ NMR and/or UV/Vis spectroscopies. It was postulated that these aggregates might directly participate in the aldol reaction.[15] This hypothesis was supported by the high dissociation barriers of the lithium oligomers ($>15.5\ kcal\,mol^{-1}$ for 4-fluoroacetophenone and acetophenone cubic tetrameric lithium enolates)[16] and also by the different diastereoselectivities observed experimentally in alkylation reactions of aggregates or "naked" enolates.[17] However, it is known that lower aggregates of several types of organolithium species are more reactive than higher ones.[18] Consequently, due to the complexity of these aggregates and the possibility of interconversion between them, it was suggested that lithium enolate oligomers can react by themselves or they can release monomeric or lower-order units, which are the real reactive species.[19] Very recently, Reich et al.[16] have reported an outstanding work on the aldol reaction between acetophenones and benzaldehydes in the presence of lithium diisopropylamide (LDA). These authors found that dimeric LDA reacts with acetophenone **1-H** to form a heterodimeric species **2**, which in turn gives rise to homodimers **(1-Li)$_2$** (Scheme 1). These

[a] O. Larrañaga, Dr. A. de Cózar, Dr. R. Zangi, Prof. Dr. F. P. Cossío
Departamento de Química Orgánica I/
Kimika Organikoa I Saila, Facultad de Química/
Kimika Fakultatea Euskal Herriko Unibertsitatea
UPV/EHU and Donostia International Physics Center (DIPC)
1072, 20018 San Sebastián–Donostia (Spain)
E-mail: fp.cossio@ehu.es

[b] Dr. A. de Cózar, Dr. R. Zangi
IKERBASQUE, Basque Foundation for Science
48011 Bilbao (Spain)

[c] Dr. A. de Cózar, Prof. Dr. F. M. Bickelhaupt
Department of Theoretical Chemistry and
Amsterdam Center for Multiscale Modeling (ACMM)
VU University Amsterdam 1083
1081HV Amsterdam (The Netherlands)

[d] Prof. Dr. F. M. Bickelhaupt
Radboud University Nijmegen, Heyendaalseweg 135
6525 AJ Nijmegen (The Netherlands)
Fax: (+34) 943015270

Supporting information for this article is available on the WWW under http://dx.doi.org/10.1002/chem.201301597.

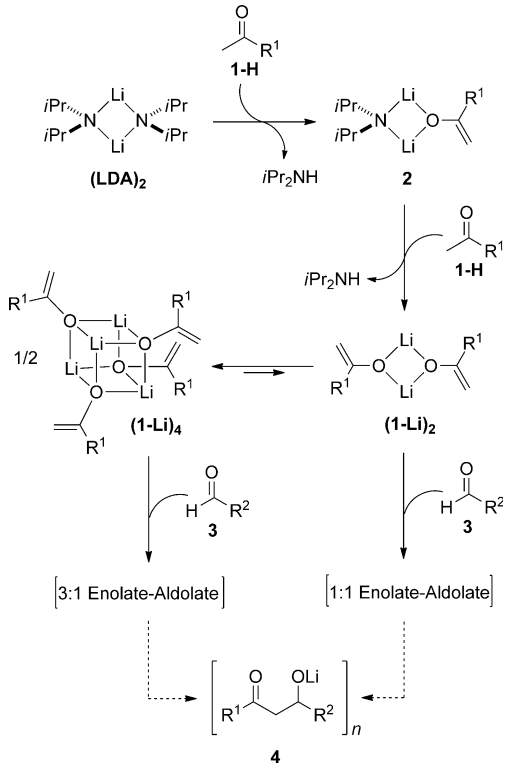


Scheme 1. Aldol reaction between ketones **1-H** and aldehydes **3** promoted by LDA, according to Reich et al. (see ref. [20]). Solvation around the lithium centers has been omitted.

latter species dimerize to yield the corresponding tetramers **(1-Li)$_4$**, which are thermodynamically more stable than dimers **(1-Li)$_2$**. Both metastable homodimer **(1-Li)$_2$** and the corresponding tetramer **(1-Li)$_4$** were characterized by NMR spectroscopy and found to be able to react with aromatic aldehydes to yield the corresponding 1:1 and 3:1 enolate–aldolate complexes. The dimer was about 17 times more reactive than the corresponding tetramer. According to these authors, the 3:1 enolate–aldolate species reacts about 2.3 times faster than **(1-Li)$_4$** and no other intermediate enolate–aldolate complexes were detected by using $^{19}$F NMR spectroscopy. Interestingly, the authors[16] pointed out that "a scheme where the 3:1 adduct dissociates unimolecularly to lower aggregates before reacting with aldehyde does not fit the kinetic traces".

These experimental results suggest that in the tetrameric species subsequent aldol reactions take place faster than the first one. This idea is interesting within a wider context, since allosteric effects are well-known in proteins like hemoglobin and other enzymes[20] as well as in complex catalysts.[21] However, the nature of the positive cooperative effects in lithium aggregates is unknown and difficult to assess experimentally.

Another important issue is the nature of the transition structures associated with aldol reactions.[22] Both acyclic[23] and cyclic transition structures have been postulated. The latter occur through mechanisms similar to [3,3]-sigmatropic suprafacial reactions (metallo-Claisen mechanism,[24]

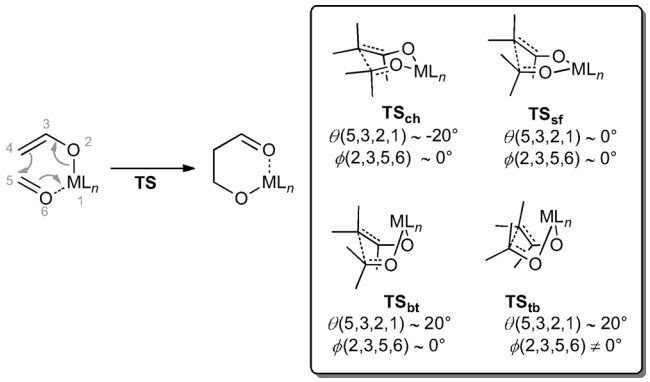


Figure 1. Postulated cyclic transition structures associated with aldol reaction. Subscripts ch, sf, bt, and tb stand for chair, sofa, boat and twist-boat, respectively. Approximate dihedral angles (in absolute value) associated with each transition structure are also indicated.

Figure 1). These cyclic transition structures can in turn be of chair **TS$_{ch}$** (the well-known Zimmerman–Traxler[25] model), sofa **TS$_{sf}$**,[26] boat **TS$_{bt}$**,[27] twist-boat **TS$_{tb}$**[28] (Figure 1), or pseudo-[3+2][29] type. In the case of lithium enolates, computational studies carried out on model systems[22,30,31] and experimental evidences obtained from deuterium-labeled enolates[32] suggest that sofa transition states **TS$_{sf}$** are the preferred ones.

On the basis of these previous results, we have investigated the model aldol reactions of monomeric, dimeric, and tetrameric lithium enolates to analyze the structure and reactivity of these nucleophiles. In particular, our aim has been to assess the origins of the distinct kinetic behavior of the different aggregates as well as the nature of the transition states depending upon the aggregation state. The ultimate goal of this work is to assess the possibility of cooperative effects in the successive aldol reactions, whose existence has been suggested by previous experimental work. Given the elusive nature of the different species, computational tools appear to be especially well-suited for these purposes.

## Results and Discussion

**Monomeric, dimeric, tetrameric, and hexameric aggregates of lithium enolates**: We started our study analyzing computationally the main features of the monomeric, dimeric, and tetrameric aggregates of lithium enolates derived from acetaldehyde **1a-H** and acetone **1b-H** (Scheme 2). These calculations were performed in the presence of dimethylether (DME) molecules to saturate the coordination sphere of lithium cation. In good agreement with the results obtained by Pratt et al.,[33] kinetically stable structures were obtained for the different aggregates (Figure 2).

The results collected in Figure 2 indicate that the main geometric features of the different aggregates of acetaldehyde and acetone are quite similar to each other. However, a slight increase in the O–Li distances was found on going from lower to higher aggregates, as it can be seen by inspec-

  

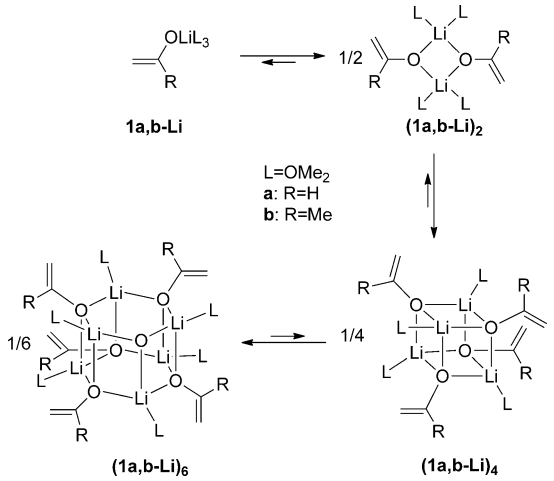


Scheme 2. Oligomers derived from monomeric enolates **1a**,**b-Li**.

tion of the average values $\langle R_{OLi}\rangle$reported in Figure 2. Similarly, the charges of the oxygen and lithium atoms were found to increase from lower to higher aggregates. We can define the average absolute charge value of the aggregate with $2n$ point charges within $Li_nO_n$ clusters as Equation (1), in which $q_{Li,i}$ and $q_{O,j}$ are the natural bond orbital (NBO) charges of the lithium and oxygen atoms present in each aggregate (see the Supporting Information).

$$\langle q_{OLi}\rangle = (2n)^{-1}\left[\sum_{i=1}^{n} q_{Li,i} - \sum_{j=1}^{n} q_{O,j}\right] \quad (1)$$

According to Equation (1), we can observe that the magnitude of this parameter increases in the sequence monomer < dimer < tetramer (Figure 2) thus showing a larger ionic character (i.e., $\langle q_{OLi}\rangle$values closer to +1).

We also investigated the preferred structure of lithum enolate hexamers under different conditions. Given the size of the resulting structures and the similarities found for the dimers and tetramers of **1a,b-H**, we calculated the structures of the hexamers for acetaldehyde **1a-H**. The results obtained are gathered in Figure 3. For the non-solvated structures two local minima were located. The first one corresponds to a distorted bicubic geometry for the $Li_6O_6$ core and is denoted as cubic (*c*) in Figure 3. The other one exhibits a hexagonal-prismatic (*h*) structure and was found to be about 6 kcal mol$^{-1}$ more stable than the former. Hexagonal prismatic structures have been reported for non-solvated hexamers of lithium enolates of isobutyrophenone[34] and pinacolone.[35] When we tried to optimize the fully $Me_2O$-solvated hexameric structures only the hexagonal-prismatic geometry **(1a-Li)$_6$** was obtained starting from both structures (Figure 3). This latter structure is similar to THF-solvated geometries obtained by Pratt et al.[33]

We postulated that bonding within the $Li_nO_n$ clusters should have a significant ionic character. To test this hypothesis we measured the sign of the Laplacian of electron density at the O–Li bond critical point of electron density of **1a-Li** and **(1a-Li)$_2$**. As noted by Bader and Cremer,[36] this

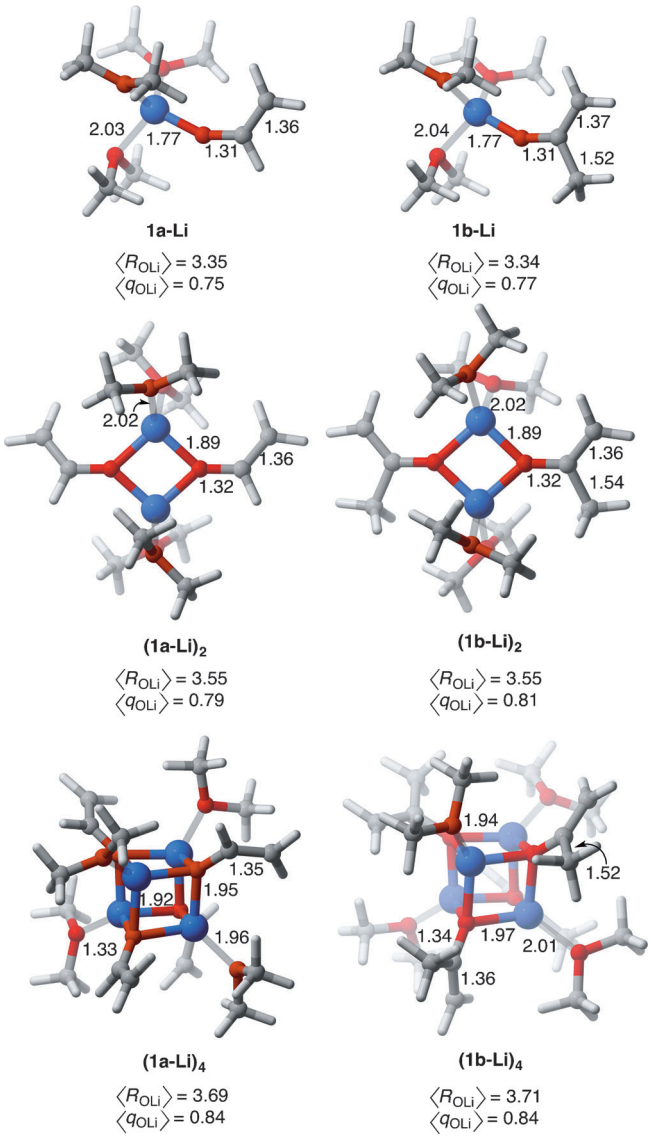


Figure 2. Fully optimized structures (B3LYP/6-31+G(d,p) level of theory) of (**1a**,**b-Li**)$_n$ ($n$=1,2,4). Distances are given in Å. Average O–Li distances $\langle R_{OLi}\rangle$ are given in a.u. Average charges $\langle q_{OLi}\rangle$ (in a.u.) are defined by Equation (1). Elements are represented as follows: hydrogen: white; carbon: gray; oxygen: red; lithium: violet.

magnitude has the dimensions of an energy density, and a positive value indicates an ionic bond. For both parent structures we obtained $\nabla^2\rho(r_c) = +0.286$ and $\nabla^2\rho(r_c) = +0.181$, respectively (both values in a.u.), thus confirming the significant ionic nature of these $Li_nO_n$ clusters. This fits in with a more general picture also found in corresponding $Li_nE_n$ clusters of methyllithium (E = C) and other lithium–element aggregates (E = H, F, Cl).[37] Already $Li_nC_n$ clusters, although less polar than the present $Li_nO_n$ cores, were shown to be held together not only by a covalent component but also by sizable electrostatic interactions.

To obtain the relative energies associated with the oligomerization reactions of lithium enolates derived from **1a,b-H**, we calculated the internal and Gibbs free energies associated with the following Equations (2) and (3), in

  

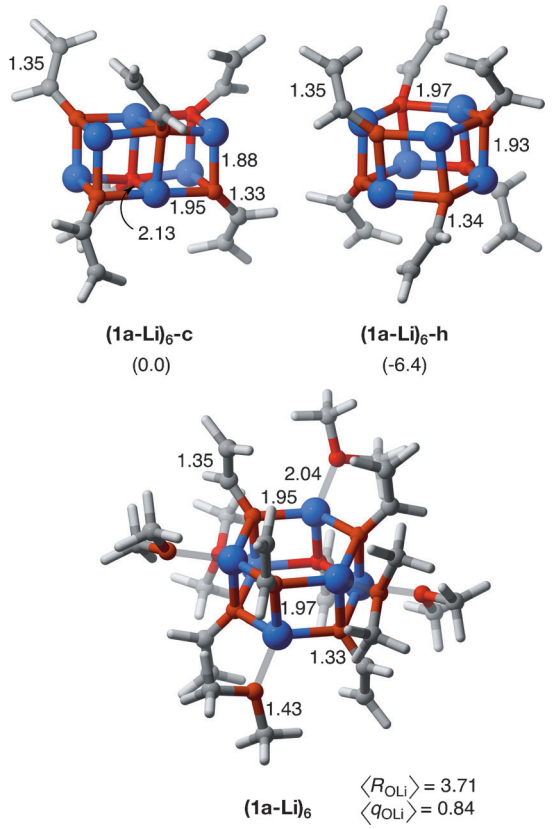


Figure 3. Fully optimized structures of different (**1a-Li**)$_6$ complexes. See the caption of Figure 2 for further details. Relative energies are given in kcal mol$^{-1}$ and were calculated at the M06/6-31+G(d,p)//B3LYP/6-31+G(d,p)+ΔZPVE level of theory.

which $\Delta m$ is the stoichiometric correction of the products with respect to the reactants [See Eq. (16) in the Computational Methods section].

$$2\,\mathbf{1a,b\text{-}Li} \rightarrow (\mathbf{1a,b\text{-}Li})_2 + 2\,Me_2O \quad (\Delta m = +1) \tag{2}$$

$$2\,(\mathbf{1a,b\text{-}Li})_2 \rightarrow (\mathbf{1a,b\text{-}Li})_4 + 4\,Me_2O \quad (\Delta m = +3) \tag{3}$$

In the case of the formation of hexamers, the following transformation in Equation (4) can be envisaged.

$$3/2\,(\mathbf{1a,b\text{-}Li})_4 \rightarrow (\mathbf{1a,b\text{-}Li})_6 \quad (\Delta m = -1/2) \tag{4}$$

Although the geometries provided by B3LYP functional are reliable enough for these systems,[38] a more adequate treatment of energies (in particular dispersion energies) is required to estimate reaction energies associated with Equations (2)–(4). In this respect M06 functional provides reliable calculations of dispersion energies, especially in highly branched systems.[39] Therefore, we used a combined M06//B3LYP approach in the evaluation of most relative energies along this work. The values obtained for acetaldehyde and acetone at the M06/6-31+G(d,p)//B3LYP/6-31+G(d,p) level of theory in vacuo and in $Et_2O$ solution are gathered in Table 1. Given the size of the structures involving acetone **1b-H** and the similarities obtained for lower aggregates, the thermodynamic data corresponding to the hexamer were computed only for acetaldehyde **1a-H**.

Table 1. Reaction energies[a] [$\Delta E$, in kcal mol$^{-1}$] and Gibbs reaction energies[a,b] [$\Delta G$, in kcal mol$^{-1}$] associated with Equations (2)–(4).

| | $\Delta E$ $\varepsilon=1.00$ | $\Delta E$ $\varepsilon=4.20$[c] | $\Delta G$ $\varepsilon=1.00$ | $\Delta G$ $\varepsilon=4.20$[c] |
|---|---|---|---|---|
| $2\,\mathbf{1a,b\text{-}Li} \rightarrow (\mathbf{1a,b\text{-}Li})_2 + 2\,Me_2O$ | | | | |
| **1a-H** | −14.0 | −10.2 | −21.6 | −20.4 |
| **1b-H** | −16.5 | −13.5 | −13.5 | −22.2 |
| $2\,(\mathbf{1a,b\text{-}Li})_2 \rightarrow (\mathbf{1a,b\text{-}Li})_4 + 4\,Me_2O$ | | | | |
| **1a-H** | +4.2 | +3.8 | −20.6 | −26.6 |
| **1b-H** | +2.3 | +2.2 | −21.6 | −30.6 |
| $3/2\,(\mathbf{1a,b\text{-}Li})_4 \rightarrow (\mathbf{1a,b\text{-}Li})_6$ | | | | |
| **1a-H** | −15.9 | −12.7 | −4.25 | −0.1 |

[a] Values computed at the M06/6-31+G(d,p)//B3LYP/6-31+G(d,p) level. [b] Values computed at 298 K. [c] Values computed by using the self-consistent reaction field PCM model in diethyl ether.

These results indicate that tetramers and hexamers should be the major species in solution, followed by the dimers, which is in good agreement with previous computational and experimental work on related systems. To assess the reactivity of these lithium aggregates in subsequent aldol reactions, we have computed the chemical potential, hardness, and nucleophilicity (both global and local) of monomeric, dimeric, tetrameric, and hexameric species derived form **1a,b-H**. The results have been collected in Table 2 and indicate that the nucleophilicities follow the sequence monomer ≫ dimer > tetramer. The nucleophilicites of the α-carbon enolate moieties follow the same trend (see Figure S1 of the Supporting Information for a more detailed discussion). Therefore, a decreasing reactivity with increasing aggregation states should be expected for these reactions, with acetaldehyde lithium enolate oligomers being significantly more reactive than acetone analogues.

Table 2. Hardnesses[a,b] ($\eta$), chemical potentials[a,c] ($\mu$), nucleophilicities[a,d] ($\omega^-$), and local nucleophilicities of the α carbon[a,e] ($\omega^-_{C(\alpha)}$) of monomeric-, dimeric-, and tetrameric lithium aggregates of acetaldehyde **1a-H** and acetone **1b-H**.

| Species | $\eta$ [hartree] | $\mu$ [hartree] | $\omega^-$ [kcal mol$^{-1}$] | $\omega^-_{C(\alpha)}$ [kcal mol$^{-1}$] |
|---|---|---|---|---|
| **1a-Li** | 0.237 | −0.036 | 6.76[f] | 3.10[f] |
| **(1a-Li)$_2$** | 0.197 | −0.083 | 2.86[f] | 0.67[f] |
| **(1a-Li)$_4$** | 0.105 | −0.084 | 2.63[f] | 0.33[f] |
| **(1a-Li)$_6$** | 0.206 | −0.087 | 2.60[f] | 0.21[f] |
| **1b-Li** | 0.204 | −0.204 | 2.90[g] | 1.88[g] |
| **(1b-Li)$_2$** | 0.199 | −0.068 | 1.89[g] | 0.45[g] |
| **(1b-Li)$_4$** | 0.200 | −0.085 | 1.13[g] | 0.16[g] |
| **(1b-Li)$_6$** | 0.175 | −0.101 | 0.73[g] | 0.06[g] |

[a] Computed at the B3LYP/6-31+G(d,p) level. [b] Computed using Equation (20). [c] Computed using Equation (19). [d] Computed using Equation (18). [e] Computed using Equation (21). [f] Computed with respect to formaldehyde **1c** ($\eta$=0.218 hartree, $\mu$=−0.172 hartree, $\omega^+$=43.82 kcal mol$^{-1}$). [g] Computed with respect to acetone **1b-H** ($\eta$=0.231 hartree, $\mu$=−0.142 hartree, $\omega^+$=27.21 kcal mol$^{-1}$). Electrophilicities $\omega^+$computed using Equation (17).

Our calculations are in agreement with previous computational and experimental results on the geometries of lithium enolates, but do not provide any insight on the reasons underlying the structural features of the different aggregates. In other words, we can describe properly what has been observed but at this point we do not understand why these aggregates and geometries (and not others) have been obtained. Assuming the important ionic character previously described, we can estimate the electrostatic potential generated by a given $Li_nO_n$ aggregate $a$ possessing an specific geometry $g$, according to Equation (5)

$$E_{a,g}^{\mathrm{Coul}} = \sum_{i=1}^{n}\sum_{j>i}^{n}\frac{q_i q_j}{R_{i,j}} \qquad \text{(in a.u.)} \tag{5}$$

If we average the distances and charges according to Equation (1) (see Figures 2 and 3), then we can approximate this potential energy in the form of Equation (6):

$$E_{a,g}^{\mathrm{Coul}} \approx \frac{\langle q_{\mathrm{OLi}}\rangle^2}{\langle R_{\mathrm{OLi}}\rangle}\sum_{i=1}^{n}\sum_{j>i}^{n}V_{i,j} = \frac{\langle q_{\mathrm{OLi}}\rangle^2}{\langle R_{\mathrm{OLi}}\rangle}V_{a,g} \tag{6}$$

In Equation (6), $V_{a,g}$is a normalized electrostatic potential for which we make $q(\mathrm{Li}) = |q(\mathrm{O})| = R_{\mathrm{OLi}} = 1$.

For ideal symmetric aggregates $a$ with specific geometries $g$, we can estimate the corresponding $V_{a,g}$ values analytically. In the case of the monomer, only a linear arrangement is possible and we obtain $V_{m,l} = -1$ a.u.

If we consider a dimer with a linear $C_{\infty V}$ symmetry (Figure 4), we obtain the following expressions given in Equation (7) and therefore $V_{d,l} = -7/3 \approx 2.33$ a. u.

$$\begin{aligned} V_{1,2} &= V_{2,3} = V_{3,4} = -1 \\ V_{1,3} &= V_{2,4} = +1/2 \\ V_{1,4} &= -1/3 \end{aligned} \tag{7}$$

In the case of a $D_{2h}$-symmetric square-planar dimer (Figure 4), the identities in Equation (8) are readily obtained and the total normalized electric potential is $V_{d,s} = 2\left[\left(1/\sqrt{2}\right) - 2\right] \approx -2.59$ a.u.

$$\begin{aligned} V_{1,2} &= V_{1,4} = V_{2,3} = V_{3,4} = -1 \\ V_{1,3} &= V_{2,4} = +1/\sqrt{2} \end{aligned} \tag{8}$$

This result indicates that the square-planar arrangement is more stable than the linear one. If we consider a tetrahedral arrangement, it is found that $V_{d,t} = -2$ a.u. Therefore, the tetrahedral geometry for the $Li_2O_2$ cluster is the less-favored one from a Coulombic standpoint. This is not surprising since this geometry forces two pairs of identical charges to approach each other (See Figure 4). Similarly, it can be readily seen that for odd oligomers (trimers, pentamers) 3D-prismatic geometries are not stable because of repulsive interactions.

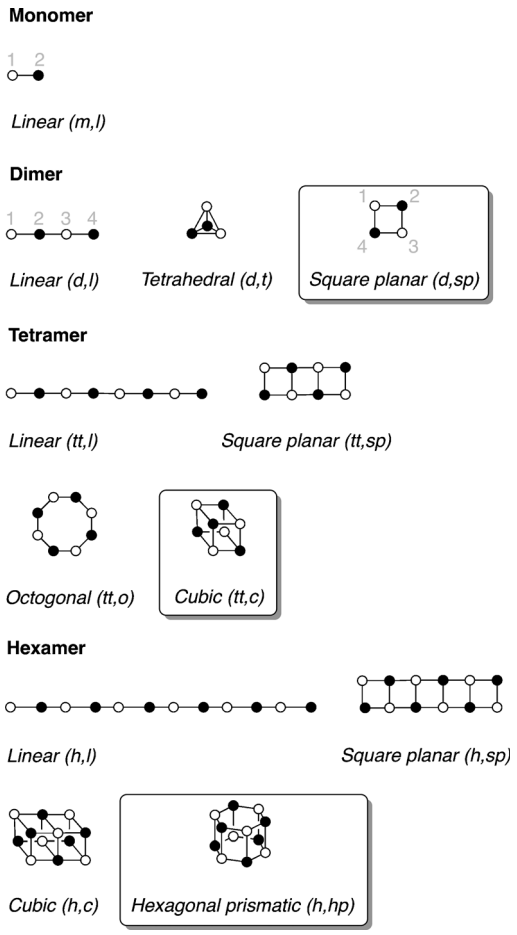


Figure 4. Model geometries for alternating positive and negative charges in monomeric, dimeric, tetrameric, and hexameric aggregates. Arrangements for which X-ray diffraction structures have been reported have been highlighted.

We can define the stabilization energy with respect to the monomer as Equation (9):

$$\Delta V_{a,g} = -V_{a,g} - n \tag{9}$$

According to this definition, the stabilization energy per point charge is simply Equation (10):

$$\Delta \bar{V}_{a,g} = \frac{\Delta V_{a,g}}{2n} \tag{10}$$

Therefore, for a dimeric tetrahedral arrangement we obtain $\Delta V_{d,t} = 0$. Following a similar procedure, we have obtained different $V_{a,g}$, $\Delta V_{a,g}$, and $\Delta \bar{V}_{a,g}$values for the respective aggregates and geometries. The details can be found in the Supporting Information and the results have been collected in Table 3.

These results indicate that for tetramers and hexamers the linear arrangements are the least favored ones. In the case of the dimer, the most stable structure is square planar, which is in good agreement with the experimental evidence. Similarly, tetramers find their strongest Coulombic stabilization through cubic arrangements, a result also in agreement

  

Table 3. Normalized potentials[a] ($V_{a,g}$, in a.u.), approximate Coulombic potentials[a,b] ($E^{Coul}_{a,g}$, in a.u.), stabilization energies with respect to the monomer[c] ($\Delta V_{a,g}$, in a.u.) and stabilization energies per point charge[d] ($\Delta\bar{V}_{a,g}$, in a.u.) for different model aggregates and geometries[e] associated with alternating point charges.[f]

| Aggregate ($n$) | Geometry | $E^{Coul}_{a,g}$ | $\Delta V_{a,g}$ | $\Delta\bar{V}_{a,g}$ |
|---|---|---|---|---|
| monomer ($n$=1) | linear | −1.00 (−0.17) | 0.00 | 0.00 |
| dimer ($n$=2) | linear | −2.33 | 0.33 | 0.08 |
| | tetrahedral | −2.00 | 0.00 | 0.00 |
| | *square planar* | *−2.59 (−0.44)* | *0.59* | *0.15* |
| tetramer ($n$=4) | linear | −5.07 | 1.07 | 0.13 |
| | octagonal | −5.45 | 1.45 | 0.18 |
| | square planar | −5.58 | 1.58 | 0.20 |
| | *cubic* | *−5.82 (−0.80)* | *1.82* | *0.23* |
| hexamer ($n$=6) | linear | −7.83 | 1.83 | 0.15 |
| | square planar | −8.58 | 2.58 | 0.21 |
| | cubic | −9.00 | 3.00 | 0.25 |
| | *hexagonal prismatic* | *−8.90 (−1.69)* | *2.90* | *0.24* |

[a] Computed by means of Equation (6). [b] $E^{Coul}_{a,g}$ energies computed by using the $\langle q_{OLi}\rangle$ and $\langle R_{OLi}\rangle$ values reported in Figures 2 and 3. [c] Computed according to Equation (9). [d] Computed according to Equation (10). [e] Geometries and numbers highlighted in italics correspond to arrangements that have been observed experimentally by using X-ray diffraction for different compounds. [f] See Figure 4 and the Supporting Information for further details.

with the X-ray and NMR data.[40] Hexamers, however, yield two structures very close in Coulombic energy: the fused-cubic and the hexagonal-prismatic arrangements. Actually, the former is more stable than the latter in terms of electrostatic potential energy. In the case of the non-solvated structure of **(1a-Li)$_6$**, we found a geometry of this type (See Figure 3), although it was computed to be about 6 kcal mol$^{-1}$ less stable than the hexagonal-prismatic one, which turns out to be the only viable solvated structure. These combined results point to a preference for the hexagonal-prismatic arrangement because of the contribution of covalent[40] and non-electrostatic non-bonding interactions. In addition, tetrahedral coordination around the lithium atom is not favored for the lithium atoms incorporated into the fused part of the cubic arrangement, thus resulting in the exclusive formation of hexagonal-prismatic structures.

As far as the electrostatic stabilization energies for the different aggregates are concerned, our results suggest that most likely the hexagonal-prismatic hexamer represents an upper limit in terms of stabilization energy per point charge $\Delta\bar{V}_{a,g}$. In addition, as we have commented before, in the case of odd oligomers the regular prismatic geometries are not favored and therefore only polygonal (for trimers) and fused square-planar (ladder) structures are viable, especially in the case of solvated oligomers, as suggested by Collum et al. for lithium phenolates.[41] Probably, cyclic-planar dimers and cubic tetramers represent the optimal aggregation/geometry combination for partially ionic $Li_nO_n$ clusters. Such arrangements have been shown in $Li_nC_n$ clusters to gain much stability through direct covalent Li−Li bonding.[42]

**Aldol reactions involving monomeric enolates**: To assess the intrinsic reactivity of monomeric lithium enolates, we analyzed the effect of lithium coordination on unsolvated enolate **1a-Li′**. Since in these model calculations only the intrinsic variation of the relative energies along the C4−C5 distances were assessed, these calculations were performed at the M06/6-31+G**B3LYP/6-31+G** level in the absence of solvent effects. We approached both reactants through three different arrangements. In the first one, denoted as Scan 1 in Figure 5, the lithium cation is attached only to formaldehyde. In this case, the reactants converge to the aldol adduct

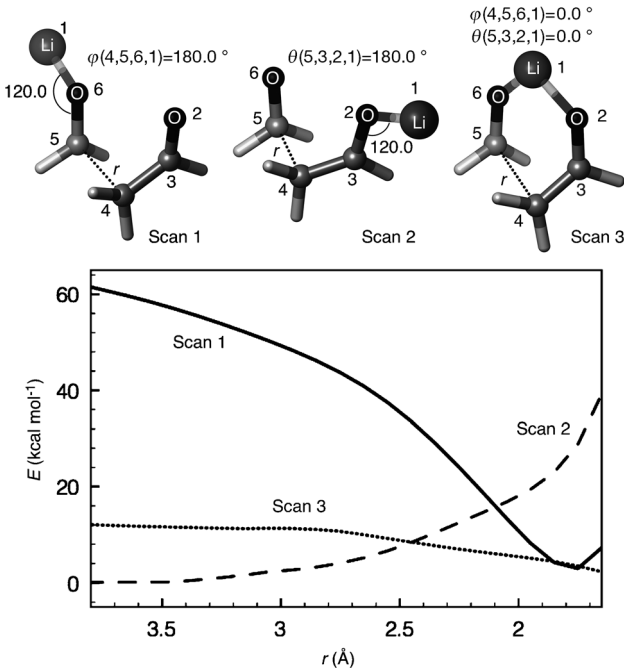


Figure 5. Relaxed scans (M06/6-31+G**//B3LYP/6-31+G** level) associated with the interaction between unsolvated enolate of acetaldehyde and formaldehyde at different C3−Cb distances $r$ in the presence of a lithium cation. Frozen bond lengths and dihedral angles are given in Å and ° respectively.

through a downhill process. Along the second approach (Scan 2, Figure 5), the lithium is bound only to the oxygen atom of the enolate. In line with the relatively weaker nucleophilicity of the **1a-Li′** species (see above), this process is uphill and the aldol adduct is of higher energy than the separated reactants. Finally, in the case of Scan 3 (Figure 5), lithium coordination to both the enolate and the electrophile was allowed thus resulting in a profile similar to (but less pronounced than) that found for Scan 1.

Therefore, aldol reactions involving cyclic intermediates and transition structures should be the preferred ones since these cyclic reaction paths encompass the stability of the lithium enolate (at the cost of a lower nucleophilicity) and

  

that of the corresponding carbonyl compound. In the case of this latter partner, the electrophilicity enhancement induced by the metal is actually the driving force of the whole process.

When the solvated structures were considered, a behavior similar to that observed in Figure 5 was observed. Interaction between **1a-Li** and formaldehyde **1c-H** requires the formation of intermediate ***m*-INT1a** through exchange with one coordinated $Me_2O$ molecule, which is an almost energetically neutral elementary process. From this intermediate, aldol adduct ***m*-P1a** was obtained in an exergonic step (Figure 6). We were unable to locate a transition structure

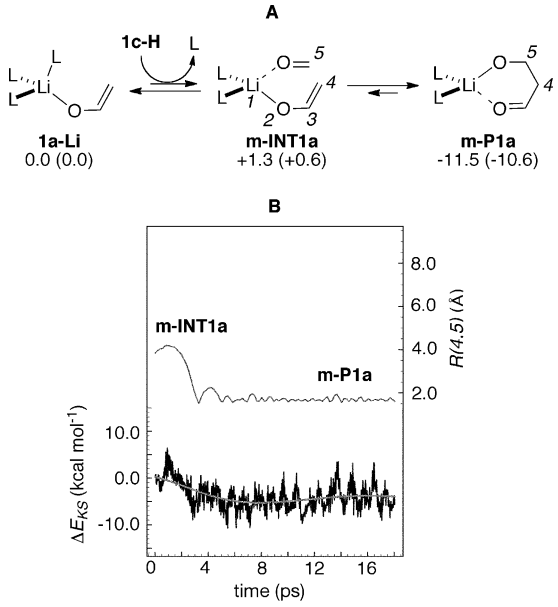


Figure 6. A) Reaction between solvated monomeric **1a-Li** (L = $OMe_2$) and formaldehyde **1c-H**. Numbers correspond to relative energies and Gibbs energies (in parentheses, kcal mol$^{-1}$), computed at 220.15 K, at the M06(PCM=$Et_2O$)/6-31+G**//B3LYP/6-31+G** level of theory; B) Car–Parrinello molecular dynamics (CPMD) simulation at 220.15 K showing spontaneous conversion of ***m*-INT1a** into ***m*-P1a**.

connecting ***m*-INT1a** and ***m*-P1a**, as we observed in the scans involving the unsolvated structures. To check if the former intermediate was actually a fleeting species,[43] we performed Car–Parrinello molecular dynamics (CPMD) simulations and observed the spontaneous transformation of ***m*-INT1a** into the corresponding aldol adduct ***m*-P1a**. Thus, Figure 6B reveals a barrierless formation of the C4–C5 bond in a few picoseconds.

Since formaldehyde is an exceptionally strong electrophile among carbonyl compounds, we repeated the same study on solvated monomeric enolate **1b-Li** and acetone **1b-H**. In this case, a saddle-point ***m*-TS1b** was located, although with a quite low associated activation energy. CPMD simulations on ***m*-INT1b** (Figure 7B) yielded very variable distances between C4 and C5 but without formation of a C4–C5 bond, thus showing the kinetic persistence of this reactive intermediate, which is almost isoenergetic with respect to mono-

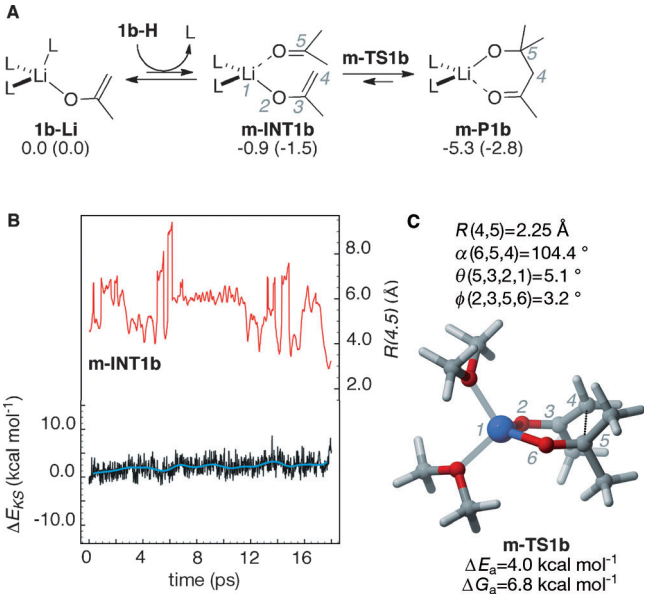


Figure 7. A) Reaction between solvated monomeric **1b-Li** (L = $OMe_2$) and acetone **1b-H**. Numbers correspond to relative energies and Gibbs energies (in parentheses, kcal mol$^{-1}$), computed at 220.15 K, at the M06-(PCM=$Et_2O$)/6-31+G**//B3LYP/6-31+G** level of theory. B) Carr–Parrinello molecular dynamics (CPMD) simulation at 220.15 K showing the stability of ***m*-INT1b** as a function of time. C) Chief geometric features of saddle-point ***m*-TS1b**, optimized at the B3LYP/6-31+G** level. Distances and angles are given in Å and °, respectively. Activation energies are also reported.

meric reactant **1b-Li**. The shape of ***m*-TS1b** has a sofa geometry, which is in good agreement with the transition structures described by Houk et al.[22] with a dihedral angle $\theta$ of 5.1° and a twist dihedral angle of 3.2°. (see Figure 1 for the definition of angles).

The approaching trajectory of the enolate to the carbonyl group presents an angle α of about 104°, a value slightly smaller than that associated with the ideal Bürgui–Dunitz trajectory for an addition to a carbonyl group.[44] Although the formation of the new C–C bond is energetically favored, it is only slightly exothermic in terms of Gibbs energy.

Why does transition structure ***m*-TS1b** adopts a sofa conformation instead of a chair-like or boat conformation? To understand the reasons for this particular geometry of aldol transition structures involving this kind of lithium enolates, we performed a rigid scan on the optimized geometry of ***m*-TS1b** by varying only the dihedral angle $\theta$ (See Figures 1 and 7). The result of this scan is gathered in Figure 8.

It is readily appreciated that the most stable sofa conformation occupies a relatively flat zone for $-10 \leq \theta \leq +10°$, the boat and chair conformations being strongly destabilized for values of $\theta$ larger than $\pm 20°$ because of strong 1,4- and 1,3-diaxial van der Waals repulsive interactions.

If we estimate the electrostatic interactions between the lithium cation and the oxygen and carbon atoms involved in the cyclic transition structure, the relative Coulombic energies for different values of $\theta$ (See Figure 7 for atom ordering) can be approximated as Equation (11), in which the

  

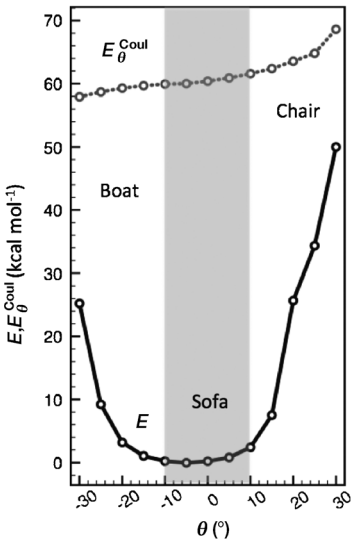


Figure 8. Scan of relative total (B3LYP/6-31+G* level of theory) and Coulombic (B3LYP/6-31+G* NBO charges) energies ($\Delta E$ and $\Delta E_\theta^{Coul}$, respectively) versus dihedral angle $\theta$ (See Figure 1 for the definition of this angle) of transition structure ***m*-TS1b**. The region occupied by the sofa conformations is highlighted in gray.

constant term $\Lambda$ stands for the following $\theta$ independent terms in Equation (12):

$$\Delta E_\theta^{Coul} \approx q_1\left[\frac{q_3}{R_{1,3}(\theta)}+\frac{q_5}{R_{1,5}(\theta)}+\frac{\bar{q}_4}{R_{1,4}(\theta)}\right]-\Lambda \quad \text{(in a.u.)} \tag{11}$$

$$\Lambda = E_{1,2}^{Coul}+E_{1,6}^{Coul}+\sum_{i=2}^{6}\sum_{j>i}^{6}\frac{q_i q_j}{R_{1,j}} \quad \text{(in a.u.)} \tag{12}$$

In Equation (11): $\bar{q}_4=-0.22$ e is the NBO combined charge of the methylene group at C4. The two Coulombic interactions between Li1 and C3 and C4 are repulsive, the respective NBO charges being +0.61, +0.53, and +0.49 a.u. For this reason, the $\Delta E_\theta^{Coul}$terms shown in Figure 9 are positive. The only stabilizing electrostatic term is the one that corresponds to the Li1–C4($H_2$) interaction. Therefore, the less destabilizing Coulombic terms are achieved for $\theta<0$, thus favoring boat conformations associated with shorter $R_{1,4}$ distances. Electrostatic interactions do not favor chair conformations associated with large $R_{1,4}$ distances and with $\theta$ values larger than +20°. Therefore, in these kind of transition structures, the sofa conformation represents an optimal trade-off between Coulombic interactions and repulsive 1,4-diaxial interactions. This electrostatic-steric model also predicts that highly nucleophilic enolates (with large negative $\bar{q}_4$ values) and small substituents at C4 and around the Li1 cationic center (which minimize repulsive 1,4-diaxial interactions) should promote a transition from sofa to boat or twist-boat conformations. Alternatively, metal–oxygen covalent interactions, which minimize the relevance of these electrostatic interactions, or adequate cyclic substitution patterns should stabilize the chair conformations, thus resulting in Zimmerman–Traxler geometries.

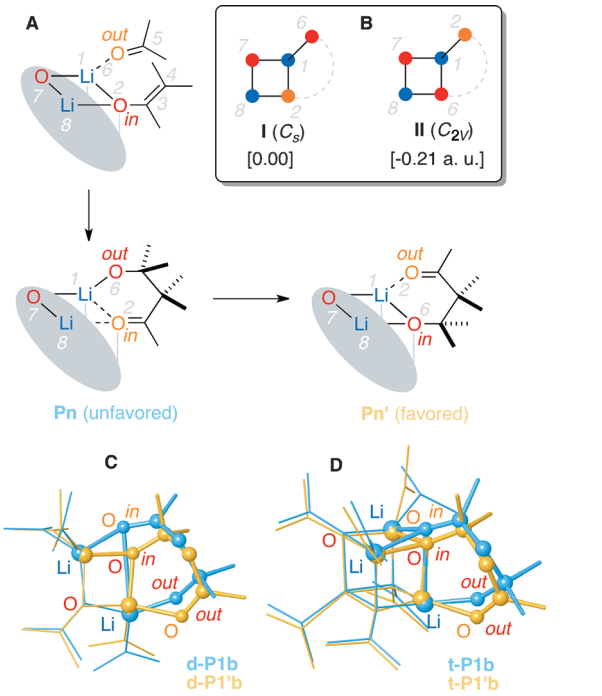


Figure 9. A) Cartoon showing the transformation of the oxygen atoms of the enolate and the carbonyl compound through aldol reactions involving $Li_nO_n$ clusters. B) Schematic representation of electrostatic distributions **I** and **II** associated with products **P*n*** and **P*n*′** respectively. The colors red and blue denote charges of −1 e and +1 e, respectively. The orange point denotes a charge of −0.5 e. The relative normalized electrostatic potentials are also indicated. C) Superimposed optimized geometries (B3LYP/6-31+G(d,p) level) of compounds **d-P1b** and **d-P1′b** showing the larger O(*in*)–Li distances in the less stable aldol product **d-P1b**. Hydrogen atoms have been omitted for the sake of clarity. D) Same as for (C) but involving tetrameric adducts **t-P1b** and **t-P1′b**.

Given that the reaction profile associated with the aldol dimerization of acetone is more similar to other stereochemically complex aldol reactions, in the following sections only reaction between oligomers **(1b-Li)$_n$** ($n$=2,4) and acetone **1b-H** will be discussed. The data corresponding to the aldol reaction between acetaldehyde and formaldehyde can be found in the Supporting Information.

**Aldol reactions involving dimeric structures**: The reaction profiles associated with the aldol dimerization of acetone **1b-H** through the dimeric enolate **(1b-Li)$_2$** are gathered in Scheme 3. Also in this case, displacement of one coordinating solvent molecule by the carbonyl compound is almost neutral from the energetic standpoint. From intermediate **d-INT1b** the first aldol product is obtained with an activation energy of about 10 kcal mol$^{-1}$, a value higher than that obtained for the monomer. This confirms the lower reactivity predicted for enolate dimer **(1b-Li)$_2$** with respect to the monomer (see above).

Our calculations indicate that formation of **d-P1b** is endothermic. According to our electrostatic model, it is clear

  

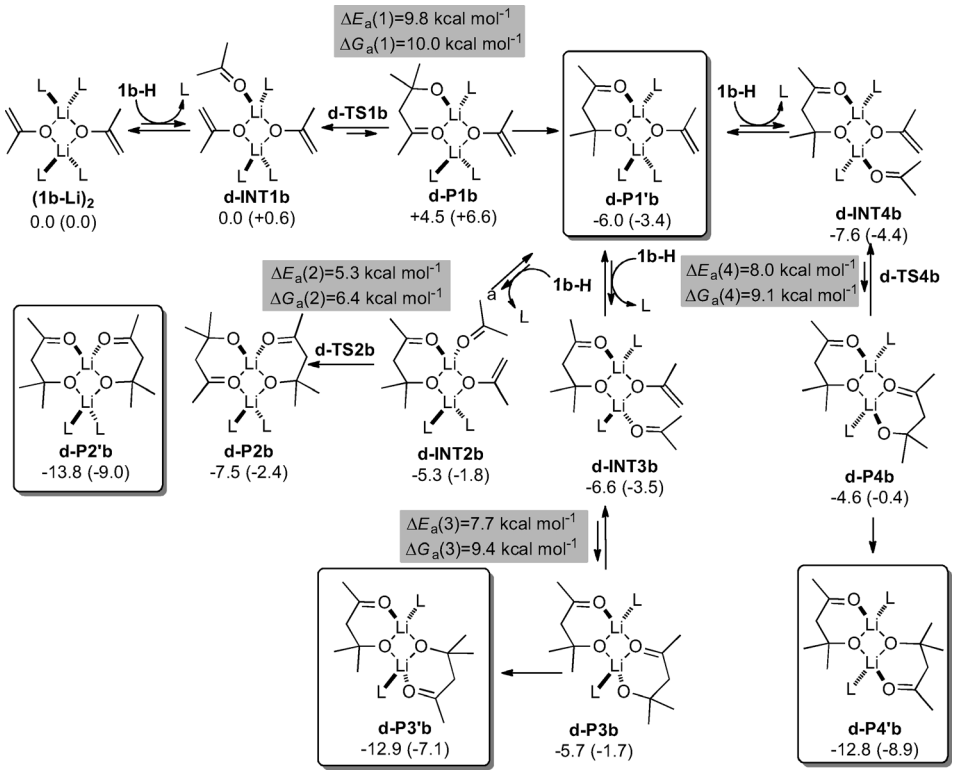


Scheme 3. Reaction profiles from the possible aldol reactions between enolate dimers **(1b-Li)$_2$** with acetone **1b-H**. Numbers below the arrows correspond to the relative energies. The corresponding relative Gibbs energies, computed at 220.15 K, are in parentheses. All results have been computed at the M06(PCM)/6-31+G**//B3LYP/6-31+G** level of theory and are given in kcal mol$^{-1}$. $\Delta E_a$ and $\Delta G_a$ are the corresponding activation energies and Gibbs energy barriers, respectively. L = $OMe_2$.

that the oxygen atom coming from the electrophilic carbonyl compound **1b-H** is converted into an alkoxide oxygen, whereas the reverse transformation takes place at the oxygen atom of the former enolate moiety. As a result, a "neutral" oxygen atom is now within the dimeric $Li_2O_2$ cluster. The alternative product, denoted as **d-P1′b** in Scheme 3, exhibits a more ionic $Li_2O_2$ cluster since in this aldol adduct the oxygen atoms associated with the enolate and alkoxide moieties are inside the dimeric $Li_2O_2$ structure. This latter aldol adduct is found to be about 10 kcal mol$^{-1}$ more stable than the former.

In principle, this situation can occur in any aldol reaction involving this type of enolate aggregates. Therefore, initially formed aldol products **P*n*** should rearrange to form the much more stable adducts **P*n*′** (Figure 9A). We tested this hypothesis by means of the normalized electrostatic potential model outlined in Equation (3). In this case, the simplified arrangements I and II (Figure 9B) correspond to aldol adducts **d-P*n*** and **d-P*n*′**, respectively. If $C_s$-symmetric arrangement I is considered, the associated normalized bicentric terms are given in Equation (13). With these values it is found that the total normalized potential is $V_I \approx -2.54$ a.u.

$$2V_{1,2} = V_{1,6} = V_{1,7} = V_{2,8} = V_{7,8} = -1$$
$$2V_{1,8} = V_{2,7} = +1/\sqrt{2}$$
$$V_{6,8} = -1/\left(1+\sqrt{2}\right)$$
$$2V_{2,6} = V_{6,7} = +1/[2sin(3\pi/8)] \quad (13)$$

A similar analysis of the $C_{2v}$-symmetric structure II, in which the alkoxide oxygen atom is within the $Li_2O_2$ cluster, yields the identities given in Equation (14) and therefore $V_{II} \approx -2.75$ a.u.

$$V_{1,2} = 2V_{1,6} = V_{1,7} = V_{2,8} = V_{7,8} = -1$$
$$V_{1,8} = V_{2,7} = +1/\sqrt{2}$$
$$V_{6,8} = -1/\left[2\left(1+\sqrt{2}\right)\right]$$
$$V_{2,6} = V_{6,7} = +1/[4sin(3\pi/8)] \quad (14)$$

On the basis of these results we conclude that in $Li_nO_n$ aggregates ($n>1$), the electrostatic interactions favor arrangements in which the oxygen atoms possessing higher charges (alkoxides and enolates) are within the cluster structure. As a consequence, the aldol adducts **P*n*** initially formed should rearrange to the more stable **P*n*′** intermediates. It is noteworthy that the actual structure of **d-P1b** shows a considerable distortion for the $Li_2O_2$ cluster, as a consequence of the lower electrostatic stabilization of this square planar dimer by the "neutral" oxygen atom associated with the starting enolate. The regular geometry is recovered in the stabilized aldol adduct **d-P1′b** (Figure 9C).

From adduct **d-P1′b** the second aldol reaction can take place by substitution of one ethereal ligand by the second equivalent of carbonyl compound **1b-H**. Three possible complexes can be formed, denoted as **d-INT2b**, **d-INT3b**, and **d-INT4b** in Scheme 3. In the former case, the second aldol reaction leads to adduct **d-P2′b** through a saddle-point **d-TS2b** with an activation barrier similar to that computed for the first C–C bond-forming step. In contrast, aldol adduct **d-P3′b**, which is about 2 kcal mol$^{-1}$ more stable than **d-P2′b**, is formed via **d-TS2b** with an activation barrier of about 3 kcal mol$^{-1}$ lower than that associated with the formation of **d-P2′b**. Finally, **d-P4′b** can be formed via **d-TS4b** with an activation barrier similar to that found for **d-TS3b** and with a reaction energy very close to that found for **d-P2′b** (Scheme 3).

We can conclude that in lithium aggregates the most stable and kinetically favored final product is associated

  

with a *cis* arrangement between the two new carbonyl groups. In addition, a positive aggregation effect is found for the second C–C bond-formation, which is found to be of lower activation energy with respect to the first aldol addition process.

The shape of energetically similar transition structures **d-TS1b**, **d-TS3b**, and **d-TS4b** were found to be very close to each other (Figure 10), with a sofa conformation similar to that found for ***m*-TS1b** (Figure 7C). However, it is noteworthy that the saddle-point **d-TS2b**, which is associated with the kinetically favored step, shows a chair-like Zimmerman–Traxler conformation dictated by the tricyclic system generated by the C–C bond being formed, the $Li_2O_2$ cluster, and the first aldol adduct.

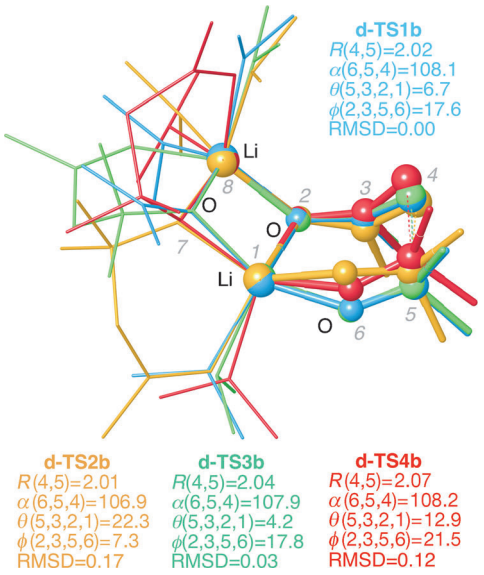


Figure 10. Superposition of fully optimized saddle-points **d-TS1b**, **d-TS2b**, and **d-TS3b** (B3LYP/6-31+G(d,p) level). RMSD: root mean square deviation values with respect to **d-TS1b**. These RMSD values were computed by considering the atoms represented in ball-and-stick mode. Distances, angles, and dihedral angles (in absolute value) are given in A and degrees, respectively. Hydrogen atoms have been omitted for the sake of clarity.

**Aldol reactions involving tetrameric structures**: Given the approximate $T_d$ symmetry of tetrameric enolate **(1b-Li)$_4$**, only one initial complex can be formed after displacement of one solvent molecule by acetone **1b-H**, denoted in Scheme 4 as **t-INT1b**. Formation of this initial complex is very close in energy with respect to the initial tetrameric aggregate. Formation of the first aldol product **t-P1b** takes place with a free activation energy of about 8 kcal mol$^{-1}$. This adduct is calculated to be approximately 4 kcal mol$^{-1}$ less stable than the reactive complex **t-INT1b**. Evolution to aldol **t-P1′b** is favored by its higher stability, derived from the insertion of the "ionic" oxygen atom coming from aldol electrophile **1b-H** into the $Li_4O_4$ cluster. In this case, the geometric constrains of the tetramer allow only a relatively low distortion of the cubic framework of **t-P1b** with respect to **t-P1′b** (Figure 9D).

From this latter stationary point different routes are possible. We have included in Scheme 4 the less-energetic one leading to the final tetrameric aldol product **t-P4′b**. The other possible kinetically unfavorable reaction paths are reported in the Supporting Information.

The second addition of **1b-H** on **t-P1′b** takes place with an activation barrier similar to that found for the first aldol process. The third and fourth aldol processes occur with increasingly lower activation energies (Scheme 4). Therefore, a positive cooperative effect in the successive aldol reactions is obtained also for the tetrameric species. The progressive stabilization of the successive aldol adducts results in the formation of tetramer **t-P4′b**, with an overall Gibbs reaction energy of about −27 kcal mol$^{-1}$ with respect to the initial tetrameric enolate **(1b-Li)$_4$**. It is noteworthy that the geometry and regiochemistry of $D_{2d}$-symmetric **t-P4′b** is similar to that found by Williard and Salvi-

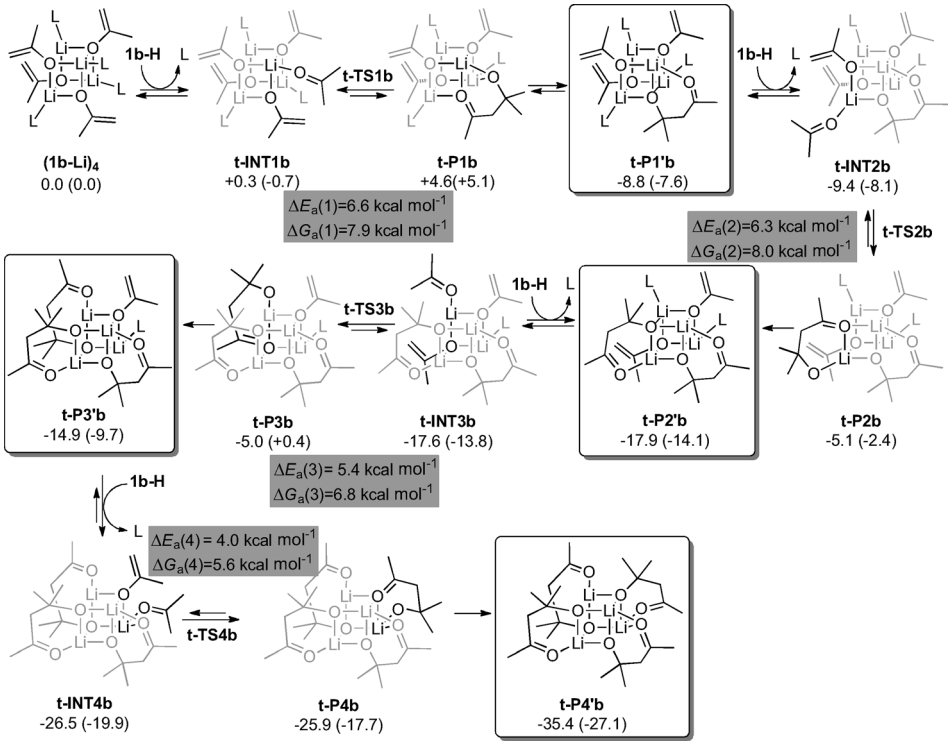


Scheme 4. Reaction profiles from the possible aldol reactions between enolate tetramers **(1b-Li)$_4$** with acetone **1b-H**. See the caption of Scheme 3 for additional details.

no[45] for the aldol reaction between pinacolone and pivaldehyde. The X-ray structure of this latter tetrameric aldol adduct presents approximate $S_4$ symmetry because of the geometric conformational constrains imposed by the *tert*-butyl groups.

In these aldol reactions involving tetrameric species the geometric features of the successive transition structures, shown in Figure 11, reveal a close similarity along the formation of the respective C4–C5 bonds. In all cases, sofa conformations were obtained after full optimization. The C4–C5 distances are of about 2 Å, which is compatible with relatively late transition structures associated with the formation of destabilized **t-P*n*b** adducts. Apparently, the combination between electrostatic interactions and geometric constrains imposed by the cubic $Li_4O_4$ cluster do not allow chair-like Zimmerman–Traxler geometries, as it occurred in the less-energetic aldol step involving dimeric structures.

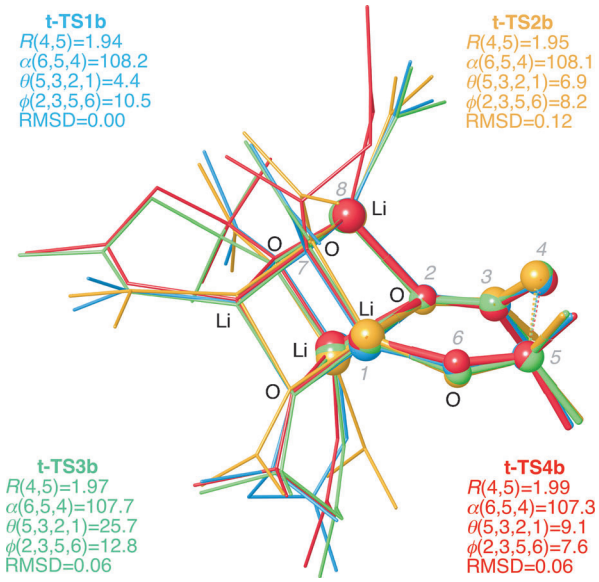


Figure 11. Superposition of fully optimized saddle-points **t-TS1b**, **t-TS2b**, **t-TS3b**, and **d-TS4b**. See the caption of Figure 10 for additional details.

## Conclusion

Our electrostatic models as well as DFT and CPMD calculations on two aldol reactions account for the main geometric features and chemical behavior of different lithium enolate aggregates. The experimentally observed square-planar and cubic geometries for dimeric and tetrameric aggregates are compatible with the maximum normalized electrostatic stabilization energies. In the case of the hexamer, for which fused cubic and hexagonal-prismatic geometries are very close in normalized electrostatic energy, the prevalence of the latter structure stems from solvation effects and, most likely, from small departures from ionic bonding. Our results also indicate that the nucleophilicity of lithium enolate aggregates decreases with the aggregation state in the order monomer $\gg$ dimer $>$ tetramer.

The role of the metallic center in aldol reactions consists mainly of enhancing the electrophilicity of the carbonyl compound, thus resulting in cyclic transition structures. In dimeric and tetrameric aggregates, formation of the new C–C bond is endergonic and results in unstable adducts in which the new alkoxide oxygen atoms lie outside the respective $Li_nO_n$ clusters. These initially formed species rearrange to form significantly more stable adducts in which the $Li_nO_n$ moieties incorporate both enolate and alkoxide oxygen atoms. Once again, electrostatics dictates these post-aldol-step transformations.

Cooperative effects are found in successive aldol reactions involving $Li_nO_n$ clusters ($n=2,4$). The first aldol step is the one that has the highest activation energy. Moreover, the first enolate forms a tighter unit with its lithium, leaving the neighboring lithium atoms less coordinated. Therefore, the remaining lithium atoms can more effectively enhance the electrophilicity of the subsequent carbonyl compounds. On the other hand, in these processes, sofa geometries are obtained for the respective transition structures in most cases, as a result of the compromise between electrostatic and van der Waals interactions.

## Computational Methods

**Computational details**: All the optimizations of stationary points along the reaction coordinates were carried out by means of Gaussian 09[46] suite of programs. The calculations were performed within the density functional theory[47] (DFT) framework. The different stationary points were optimized using the B3LYP[48] hybrid functional with the standard 6-31+G(d,p) split valence basis-set. Since B3LYP overestimates the free energy values of organolithium compounds compared to higher-level computational methods,[49] single-point calculations at the M06/6-31+G(d,p) level were performed on the fully optimized B3LYP/6-31+G(d,p) structures. This highly parameterized method is well suited for the treatment of non-bonding interactions and dispersion forces, which can be relevant in densely substituted interacting systems.[50]

Solvent effects not related to solvation of metallic centers were estimated by using the polarization continuum model[51] (PCM) method within the self-consistent reaction field (SCRF) approach.[52] Additional molecules of solvent were treated explicitly to complete the tetrahedral environment of the lithium atoms in all the studied mechanisms. All SCRF-PCM calculations were performed using diethylether ($\varepsilon=4.24$) as model solvent. In the case of the energies in solution, the standard state was established at 1 M concentrations. Therefore, at 298 K the standard correction for the 1 M standard state is shown in Equation (15):[53]

$$\Delta G^* = \Delta G^\circ - 1.9\Delta m \quad (15)$$

in which the superscripts * and ° refer to the 1 M and 1 atm states, respectively, and $\Delta m$ is the stoichiometric correction. For activation energies from two reactants to form a transition structure, $\Delta m=1$. For reaction energies this term is given by Equation (16) in which $m_i$ and $m_j$ refer to the number of equivalents of products and reactants, respectively.

$$\Delta m = \sum_i^{\text{prod}} m_i - \sum_j^{\text{react}} m_j \quad (16)$$

  

All the stationary points were characterized by harmonic vibrational analysis. Local minima showed positive definite Hessians. Fully optimized transition structures (TSs) showed one and only one imaginary frequency associated with nuclear motion along the chemical transformation under study. Reaction paths were checked by intrinsic reaction coordinate (IRC) calculations.[54]

The thermal corrections to the energy at 220.15 and 298.15 K were taken from the harmonic analyses and added to the total energies to obtain the free energies of each stationary point.

Electrophilicities ($\omega^+$) and nucleophilicities ($\omega^-$) were calculated according to the Equations (17) and (18),[55] in which, in both expressions, $\mu$ and $\eta$ denote the corresponding chemical potential and hardness,[56] respectively. These parameters were calculated by using the following approximate formulas in Equations (19) and (20),[57] in which $\varepsilon_H$ and $\varepsilon_L$ stand for the orbital energies of the HOMO and LUMO of the corresponding species, respectively.

$$\omega_A^+ = \frac{\mu_A^2}{2\eta_A} \tag{17}$$

$$\omega_A^- = \frac{(\mu_A - \mu_B)^2}{2(\eta_A + \eta_B)^2}\eta_A \tag{18}$$

$$\mu \approx \frac{\varepsilon_H - \varepsilon_L}{2} \tag{19}$$

$$\eta \approx \varepsilon_L - \varepsilon_H \tag{20}$$

Local nucleophilicities[58] $\omega_{C(\alpha)}^-$ at the alpha carbon of the enolate moieties of the different aggregates were calculated according to the following expression in Equation (21).

$$\omega_{C(\alpha)}^- = f_{C(\alpha)}^- \omega_A^- \tag{21}$$

In this expression, $f_{C(\alpha)}^-$ is the Fukui function[59] at C(α) associated with a nucleophilic attack, which in turn was calculated according to the following formula in Equation (22),[60] in which the two terms on the right part of the equation correspond to the NBO charge of the C(α) atom with $N$ and $N-1$ electrons, respectively.

$$f_{C(\alpha)}^- = q_{C(\alpha)}^-(N) - q_{C(\alpha)}(N-1) \tag{22}$$

The density-functional-theory-based Car–Parrinello[61] molecular dynamics simulations were carried out within the CPMD code[62] using the BLYP[63] gradient-corrected functional level and ultrasoft Vanderbilt[64] pseudo-potentials with a 60 Rydberg cutoff for the plane wave expansion of the orbitals. The CPMD simulations were performed at 220.15 K temperature in NVT ensembles for a total timescale of about 15 ps with a 1 fs time step for integration of equation of motion.

## Acknowledgements

O.L. gratefully acknowledges the MINECO for a predoctoral FPU grant. F.P.C., O.L. and A.d.C. gratefully acknowledge the MINECO (Grants CTQ2010-16959 and Consolider-Ingenio 2010 CSD2007-00006), the GV/EJ (Grant IT673-13) and the UPV/EHU (UFI QOSYC 11/22) for financial support. The DIPC and the SGI/IZO-SGIker UPV/EHU (European Social Fund) are gratefully acknowledged for generous allocation of computational resources. F.M.B. thanks the DIPC for financial support.

[1] *Modern Aldol Reactions, Vols. 1 and 2* (Ed.: R. Mahrwald), Wiley-VCH, Weinheim, **2004**.
[2] a) C. H. Heathcock, *Science* **1981**, *214*, 395–400; b) D. A. Evans, J. V. Nelson, T. R. Taber, *Top. Stereochem.* **1982**, *31*, 1–115; c) C. J. Cowden, I. Paterson, *Org. React.* **1997**, *51*, 1–200; d) C. Palomo, M. Oiarbide, J. Gracia, *Chem. Soc. Rev.* **2004**, *33*, 65–75.
[3] a) C. A. Wurtz, *Comp. Rend.* **1872**, *74*, 1361; b) C. A. Wurtz, *Bull. Soc. Chim. Fr.* **1872**, *17*, 436–442; c) R. J. Kane, *Ann. Physik Chem.* **1838**, *44*, 475; d) R. J. Kane, *Prakt. Chem.* **1838**, *15*, 129.
[4] B.-M. Lim, S. F. Williams, S. Massamune, in *Comprensive Organic Synthesis Vol. 2* (Eds.: B. M. Trost, I. Fleming, C. H. Heathcock), Pergamon, Oxford, **1991**, Chapters 1–7.
[5] a) B. List, in *Modern Aldol Reactions, Vol. 1* (Ed.: R. Mahrwald), Willey-VCH, Weinheim, **2004**, p. 161; b) B. List, *Acc. Chem. Res.* **2004**, *37*, 548–557; c) S. Mukherjee, J. W. Yang, S. Hoffmann, B. List, *Chem. Rev.* **2007**, *107*, 5471–5569; d) J. Zhou, V. Wakchaure, P. Kraft, B. List, *Angew. Chem.* **2008**, *120*, 7768–7771; *Angew. Chem. Int. Ed.* **2008**, *47*, 7656–7658.
[6] a) W.-D. Fessner, A. Schneider, G. Held, G. Sinerius, C. Walter, M. Hixon, J. V. Schloss, *Angew. Chem.* **1996**, *108*, 2366–2369; *Angew. Chem. Int. Ed. Engl.* **1996**, *35*, 2219–2221; b) L. J. Whalen, C.-H. Wong, *Aldrichimica Acta* **2006**, *39*, 63–71; c) T. D. Machajewski, C. H. Wong, *Angew. Chem.* **2000**, *112*, 1406–1430; *Angew. Chem. Int. Ed.* **2000**, *39*, 1352–1375.
[7] a) D. J. Kuo, I. A. Rose, *Biochemistry* **1985**, *24*, 3947–3955; b) A. Heine, L. J. G. Luz, C.-H. Wong, I. A. Wilson, *J. Mol. Biol.* **2004**, *343*, 1019–1030.
[8] F. Tanaka, C. F. Barbas III, in *Modern Aldol Reactions, Vol. 1* (Ed.: R. Mahrwald), Wiley-VCH, Weinheim, **2004**, p. 273.
[9] a) P. I. Dalko, L. Moisan, *Angew. Chem.* **2001**, *113*, 3840–3864; *Angew. Chem. Int. Ed.* **2001**, *40*, 3726–3748; b) P. I. Dalko, L. Moisan, *Angew. Chem.* **2004**, *116*, 5248–5286; *Angew. Chem. Int. Ed.* **2004**, *43*, 5138–5175; c) E. R. Jarvo, S. J. Miller, *Tetrahedron* **2002**, *58*, 2481–2700; d) A. Berkessel, H. Gröger, *Asymmetric Organocatalysis*, Willey-VCH, Weinheim, **2005**.
[10] a) J. I. Seeman, *Chem. Rev.* **1983**, *83*, 83–134; b) E. M. Arnett, F. J. Fisher, M. A. Nichols, A. A. Ribeiro, *J. Am. Chem. Soc.* **1989**, *111*, 748–749; c) E. M. Arnett, F. J. Fisher, M. A. Nichols, A. A. Ribeiro, *J. Am. Chem. Soc.* **1990**, *112*, 801–808; d) E. M. Arnett, C. A. Palmer, *J. Am. Chem. Soc.* **1990**, *112*, 7354–7360; e) G. Das, E. R. Thornton, *J. Am. Chem. Soc.* **1993**, *115*, 1302–1312; f) K. J. Kolonko, H. J. Reich, *J. Am. Chem. Soc.* **2008**, *130*, 9668–9669.
[11] R. Gareyev, J. C. Ciula, A. Streitwieser, *J. Org. Chem.* **1996**, *61*, 4589–4593.
[12] D. Seebach, *Angew. Chem.* **1988**, *100*, 1685–1715; *Angew. Chem. Int. Ed. Engl.* **1988**, *27*, 1624–1654.
[13] W. Quan, J. B. Grutzner, *J. Org. Chem.* **1986**, *51*, 4220–4224.
[14] P. G. Williard, G. B. Carpenter, *J. Am. Chem. Soc.* **1986**, *108*, 462–468.
[15] a) R. Amstutz, W. B. Schweizer, D. Seebach, J. D. Dunitz, *Helv. Chim. Acta* **1981**, *64*, 2617–2621; b) D. Seebach, R. Amstutz, J. D. Dunitz, *Helv. Chim. Acta* **1981**, *64*, 2622–2626.
[16] K. J. Kolonko, D. J. Wherritt, H. J. Reich, *J. Am. Chem. Soc.* **2011**, *133*, 16774–16777.
[17] A. Solladié-Cavallo, A. G. Csaky, I. Gantz, J. Suffert, *J. Org. Chem.* **1994**, *59*, 5343–5346.
[18] a) F. Abu-Hasanayn, A. Streitwieser, *J. Am. Chem. Soc.* **1996**, *118*, 8136–8137; b) A. Abbotto, S S.-W. Leung, A. Streitwieser, K. V. Kilway, *J. Am. Chem. Soc.* **1998**, *120*, 10807–10813; c) X. Sun, D. B. Collum, *J. Am. Chem. Soc.* **2000**, *122*, 2459–2463; d) D. B. Collum, A. J. McNeil, A. Ramirez, *Angew. Chem.* **2007**, *119*, 3060–3077; *Angew. Chem. Int. Ed.* **2007**, *46*, 3002–3017.
[19] a) A. Streitwieser, *J. Mol. Model.* **2006**, *12*, 673–680; b) C. Fressigné, J. Maddaluno, *J. Org. Chem.* **2010**, *75*, 1427–1436.
[20] J. A. Lukin, C. Ho, *Chem. Rev.* **2004**, *104*, 1219–1230.
[21] L. Kovbasyuk, R. Krämer, *Chem. Rev.* **2004**, *104*, 3161–3187.
[22] a) Y. Li, M. N. Paddon-Row, K. N. Houk, *J. Am. Chem. Soc.* **1988**, *110*, 3684–3686; b) Y. Li, M. N. Paddon-Row, K. N. Houk, *J. Org. Chem.* **1990**, *55*, 481–493.
[23] a) Y. Yamamoto, K. Maruyama, *Tetrahedron Lett.* **1980**, *21*, 4607–4619; b) R. Noyori, I. Nishida, J. Sakata, *J. Am. Chem. Soc.* **1983**, *105*, 1598–1608.
[24] D. A. Evans, L. R. McGee, *Tetrahedron Lett.* **1980**, *21*, 3975–3978.

  

[25] H. Zimmerman, M. Traxler, *J. Am. Chem. Soc.* **1957**, *79*, 1920–1923.
[26] A. Hirai, M. Nakamura, E. Nakamura, *J. Am. Chem. Soc.* **2000**, *122*, 11791–11798.
[27] a) E. Nakamura, I. Kuwajima, *Tetrahedron Lett.* **1983**, *24*, 3343–3346; b) I. Kuwajima, E. Nakamura, *Acc. Chem. Res.* **1985**, *18*, 181–187 and references cited therein.
[28] a) R. W. Hoffmann, K. Ditrich, S. Froech, D. Cremer, *Tetrahedron* **1985**, *41*, 5517–5524; b) C. Gennari, R. Todeschini, M. G. Beretta, G. Favini, C. Scolastico, *J. Org. Chem.* **1986**, *51*, 612–616.
[29] T. Anh, B. T. Thanh, *Nouv. J. Chim.* **1986**, *10*, 681–683.
[30] Y. Li, M. N. Paddon-Row, K. N. Houk, *J. Am. Chem. Soc.* **1988**, *110*, 7260.
[31] L. M. Pratt, N. V. Nguyen, B. Ramachandran, *J. Org. Chem.* **2005**, *70*, 4279–4283.
[32] C. M. Liu, W. J. Smith III, D. J. Gustin, W. R. Roush, *J. Am. Chem. Soc.* **2005**, *127*, 5770–5771.
[33] L. M. Pratt, S. C. Nguyen, B. T. Thanh, *J. Org. Chem.* **2008**, *73*, 6086–6091.
[34] M. A. Nichols, C. M. Leposa, A. D. Hunter, M. Zeller, *J. Chem. Crystallogr.* **2007**, *37*, 825–829.
[35] P. G. Williard, G. B. Carpenter, *J. Am. Chem. Soc.* **1985**, *107*, 3345–3346.
[36] a) R. F. W. Bader, *Atoms in Molecules—A Quantum Theory*, Clarendon Press, Oxford, **1990**, pp. 276–277; b) D. Cremer, E. Kraka, *Croat. Chem. Acta* **1984**, *56*, 1259–1281.
[37] a) F. M. Bickelhaupt, M.; Solà, C. Fonseca Guerra, *J. Comput. Chem.* **2007**, *28*, 238–250 Solà, C. Fonseca Guerra, *J. Chem. Theory Comput.* **2006**, *2*, 965–980; b) F. M. Bickelhaupt, M. Solà, C. Fonseca Guerra, *Faraday Discuss.* **2007**, *135*, 451–468; c) F. M. Bickelhaupt, M.; Solà, C. Fonseca Guerra, *J. Comput. Chem.* **2007**, *28*, 238–250; d) F. M. Bickelhaupt, M. Solà, C. Fonseca Guerra, *Inorg. Chem.* **2007**, *46*, 5411–5418.
[38] a) E. G. Lewars, *Computational Chemistry*, Springer, Heidelberg, **2011**; pp. 467–476; b) J. Tirado-Rives, W. L. Jorgensen, *J. Chem. Theory Comput.* **2008**, *4*, 297–306; c) S. F. Sousa, P. A. Fernandes, M. J. Ramos, *J. Phys. Chem. A* **2007**, *111*, 10439–10452.
[39] Y. Zhao, D. G. Truhlar, *Theor. Chem. Acc.* **2008**, *120*, 215–241.
[40] L. Liou, A. J. McNeil, A. Ramirez, G. E. S. Toombes, J. M. Gruver, D. B. Collum, *J. Am. Chem. Soc.* **2008**, *130*, 4859–4868.
[41] T. S. De Vries, A. Goswami, L. R. Liou, J. M. Gruver, E. Jayne, D. B. Collum, *J. Am. Chem. Soc.* **2009**, *131*, 13142–13154.
[42] F. M. Bickelhaupt, N. J. R. van Eikema Hommes, C. Fonseca Guerra, E. J. Baerends, *Organometallics* **1996**, *15*, 2923–2931.
[43] R. Hoffmann, P. von R. Schleyer, H. F. Scheffer III, *Angew. Chem.* **2008**, *120*, 7276–7279; *Angew. Chem. Int. Ed.* **2008**, *47*, 7164–7167.
[44] H. B. Burgi, J. D. Dunitz, E. Shefter, *J. Am. Chem. Soc.* **1973**, *95*, 5065–5067.
[45] P. G. Williard, J. M. Salvino, *Tetrahedron Lett.* **1985**, *26*, 3931–3934.
[46] Gaussian 09, Revision A.02, M. J. Frisch, G. W. Trucks, H. B. Schlegel, G. E. Scuseria, M. A. Robb, J. R. Cheeseman, G. Scalmani, V. Barone, B. Mennucci, G. A. Petersson, H. Nakatsuji, M. Caricato, X. Li, H. P. Hratchian, A. F. Izmaylov, J. Bloino, G. Zheng, J. L. Sonnenberg, M. Hada, M. Ehara, K. Toyota, R. Fukuda, J. Hasegawa, M. Ishida, T. Nakajima, Y. Honda, O. Kitao, H. Nakai, T. Vreven, J. A. Montgomery, Jr., J. E. Peralta, F. Ogliaro, M. Bearpark, J. J. Heyd, E. Brothers, K. N. Kudin, V. N. Staroverov, R. Kobayashi, J. Normand, K. Raghavachari, A. Rendell, J. C. Burant, S. S. Iyengar, J. Tomasi, M. Cossi, N. Rega, J. M. Millam, M. Klene, J. E. Knox, J. B. Cross, V. Bakken, C. Adamo, J. Jaramillo, R. Gomperts, R. E. Stratmann, O. Yazyev, A. J. Austin, R. Cammi, C. Pomelli, J. W. Ochterski, R. L. Martin, K. Morokuma, V. G. Zakrzewski, G. A. Voth, P. Salvador, J. J. Dannenberg, S. Dapprich, A. D. Daniels, Ö. Farkas, J. B. Foresman, J. V. Ortiz, J. Cioslowski, D. J. Fox, Gaussian, Inc. Wallingford CT, **2009**.
[47] R. G. Parr, Yang W., *Density-Functional Theory of Atoms and Molecules*, Oxford, New York, **1989**.
[48] A. D. Becke, *J. Chem. Phys.* **1993**, *98*, 5648–5650.
[49] L. M. Pratt, D. Jones, A. Sease, D. Busch, E. Faluade, S. C. Nguyen, B. T. Thanh, *Int. J. Quantum Chem.* **2009**, *109*, 34–42.
[50] a) Y. Zhao, D. G. Truhlar, *J. Chem. Theory Comput.* **2008**, *4*, 1849–1868; b) Y. Zhao, D. G. Truhlar, *Acc. Chem. Res.* **2008**, *41*, 157–167.
[51] R. Cammi, B. Mennucci, J. Tomasi, *J. Phys. Chem. A* **2000**, *104*, 5631–5637.
[52] J. Tomasi, B. Mennucci, R. Cammi, *Chem. Rev.* **2005**, *105*, 2999–3093.
[53] a) A. Ben-Naim, *Solvation Thermodynamics*; Plenum Press: New York, **1987**; b) C. P. Kelly, C. J. Cramer, D. G. Truhlar, *J. Phys. Chem. B* **2006**, *110*, 16066–16081; c) C. P. Kelly, C. J. Cramer, D. G. Truhlar, *J. Phys. Chem. B* **2007**, *111*, 408–422.
[54] a) C. González, H. B. Schelegel, *J. Chem. Phys.* **1989**, *90*, 2154–2161; b) C. González, H. B. Schelegel, *J. Phys. Chem.* **1990**, *94*, 5523–5527.
[55] P. Jaramillo, P. Pérez, R. Contreras, W. Tiznado, P. Fuentealba, *J. Phys. Chem. A* **2006**, *110*, 8181–8187.
[56] R. G. Parr, L. L. von Szentpálky, S. Liu, *J. Am. Chem. Soc.* **1999**, *121*, 1922–1924.
[57] Notice that in the valence-state parabola model, the hardness is given by $\eta=(I-A)/2$. See, for example: a) L. von Szentpály, *Chem. Phys. Lett.* **1995**, *245*, 209–214; b) L. von Szenpály, *J Phys Chem. A* **1998**, *102*, 10912–10915.
[58] P. Pérez, L. R. Domingo, M. Duque-Noreña, E. Chamorro, *J. Mol. Struct.* **2009**, *895*, 86–91.
[59] P. W. Ayers, W. Yang, L. J. Bartolotti, *The Fukui Function; in Chemical Reactivity Theory: A Density Functional View* (Ed.: P. Chattaraj), Taylor & Francis, Boca Raton, FL, **2009**, pp. 255–267, and references therein.
[60] W. Yang, W. J. Mortier, *J. Am. Chem. Soc.* **1986**, *108*, 5708–5711.
[61] R. Car, M. Parrinello, *Phys. Rev. Lett.* **1985**, *55*, 2471–2474.
[62] CPMD code (http://www.cpmd.org): Copyright MPI für Festkörperforschung, Stuttgart, and IBM Zürich Research Laboratory, 1990–2006.
[63] a) A. D. Becke, *Phys. Rev. A* **1988**, *38*, 3098–3100; b) C. Lee, W. Yang, R. C. Parr, *Phys. Rev. B* **1988**, *37*, 785–789.
[64] D. Vanderbilt, *Phys. Rev. B* **1990**, *41*, 7892–7895.

Received: April 25, 2013
Published online: August 21, 2013

  